Available online at www.sciencedirect.com
SCIENCE DIRECT®
International Journal of Heat and Fluid Flow 27 (2006) 542–550
International Journal of HEAT AND FLUID FLOW
www.elsevier.com/locate/ijhff

On the merging of turbulent spots in a supersonic boundary-layer flow

L. Krishnan, N.D. Sandham *

Aeronautics and Astronautics, School of Engineering Sciences, University of Southampton, Highfield, Southampton SO17 1BJ, United Kingdom

Available online 23 March 2006

Abstract

The complex transition flow physics associated with the merging of turbulent spots in a Mach 2 boundary-layer has been studied using direct numerical simulation. Dynamics of an isolated turbulent spot, merging of laterally displaced spots, and merging of two spots in tandem are considered. The coherent structures associated with the wingtip region of the spot are found to play a major role in destabilising the surrounding laminar fluid. In the merging of laterally displaced spots a strong velocity defect, resulting in unstable inflectional velocity profiles, is observed in the interaction zone. These local inflectional instabilities within the interaction region trigger new large scale coherent structures. During the inline merging, the calmed region behind the tail of the downstream spot is found to suppress the growth of the upstream spot. The upstream spot is ultimately engulfed by the downstream spot.

Keywords: Turbulent spots; Transition to turbulence; Compressible boundary layer; Spot merging

1. Introduction

The growth and breakdown of disturbances initiates laminar-to-turbulent transition. Large amplitude disturbances can bypass the initial linear growth stage and directly enter the non-linear growth phase. Finally, the disturbances break down into regions of intermittent turbulence in an otherwise laminar flow. Emmons (1951) named these localised islands of turbulence as 'turbulent spots'. The growth and the merger of these turbulent spots leads to fully developed turbulent flow. The length of the transition region depends on the spot creation rate and on spot growth characteristics such as the convective speed of the leading and trailing edges of the spot, lateral growth rate and interactions between spots. A schematic of a turbulent spot is depicted in Fig. 1, showing how the turbulent fluid overhangs laminar fluid at the front and sides of the spot. Behind the spot there is a region known as the calmed region (Schubauer and Klebanoff, 1955), where disturbances are low, but skin friction is higher than in the surrounding laminar boundary layer.

Narasimha (1985) reviewed the transition process and turbulent spots in a variety of flows. A classical spot photograph (Fig. 2) of Cantwell et al. (1978) reveals streaky structures in the sublayer trailing the rear interface of the spot. To date, these streaky structures were identified only in the incompressible flow visualisation studies. Earlier, Elder (1960) showed experimentally that a spot can be successfully triggered if the perturbation amplitude exceeds a critical level of about 0.2 times the free-stream velocity. He also suggested that the region of turbulent flow is the sum of the areas of individual turbulent spots. This simple superposition is possible only if the spots grow independently of each other. Savas and Coles (1985) constructed a synthetic turbulent boundary layer by triggering an array of spots in a hexagonal pattern. They suggested that the dynamics of the spot interactions are important and questioned the simple superposition of spot areas. Moreover, the recent experiments by Makita and Nishizawa (2001) showed a stronger velocity defect in the interaction zone and demonstrated that the spot merging process is different from a simple superposition of spots.

* Corresponding author. Tel.: +44 23 8059 4872; fax: +44 23 8059 3058.
E-mail addresses: krishnan@soton.ac.uk (L. Krishnan), n.sandham@soton.ac.uk (N.D. Sandham).

0142-727X/$ - see front matter © 2006 Elsevier Inc. All rights reserved.
doi:10.1016/j.ijheatfluidflow.2006.02.002

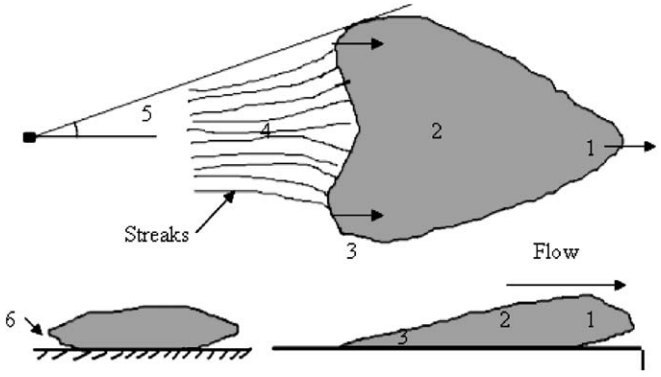

Fig. 1. Turbulent spot nomenclature: (1) front overhang, (2) turbulent core, (3) lateral wingtip, (4) calmed region, (5) lateral spreading half-angle, (6) spanwise overhang.

Fig. 2. Spot flow visualisation showing the sublayer streaks (Cantwell et al., 1978).

Direct numerical simulations (DNS) of turbulent spots in an incompressible boundary layer were presented by Henningson et al. (1987). They showed that turbulent patches embedded within an arrowhead-shaped region grow at a half-spreading angle of about 7°, with estimated front and rear convection speeds of about $0.83u_\infty$ and $0.50u_\infty$. Numerical simulation of bypass transition in an initially laminar boundary layer beneath free-stream turbulence was carried out by Jacobs and Durbin (2001). They found the near-wall streaks to be stable whereas the lifted streaks became receptivity sites for smaller scale free-stream turbulence and triggered turbulent spots. This work showed the formation of spots in flows with top–down perturbations (i.e. free-stream disturbances) in contrast to the more conventional bottom–up perturbations (caused by near-wall disturbances).

Most of the studies to date have been performed to explore the dynamics of spots in an incompressible flow. The physics associated with the spot spreading mechanism and the spot interactions are only vaguely described in the literature. A clear understanding of the transition physics is required for the design of supersonic and hypersonic vehicles, yet data for compressible spots in the literature is very limited.

Krishnan and Sandham (2004a) used DNS to show that an increase in the Reynolds number has a destabilising effect while the Mach number inhibits the growth of a single hairpin structure into a turbulent spot in a plane Poiseuille flow. The effect of compressibility on the spreading of isolated turbulent spots in a compressible boundary layer was reported by Krishnan and Sandham (2004b). They found a marked reduction in the lateral half-spreading of the spots from 5° to 1.7° with the flow Mach number varying from 2 to 6 in agreement with experiments (Fischer, 1972). Spot visualisations clearly revealed that young spots consist of an array of hairpin and quasi streamwise vortices. Spanwise-coherent structures which are connected to the supersonic modes (Mack mode) were seen under the front overhang of the spot in a Mach 6 boundary layer. Krishnan and Sandham (2004c) investigated the complex flow physics associated with the interaction of a turbulent spot with an oblique shock-induced laminar separation bubble. The passage of the spot completely collapsed the bubble in the interaction region and the lateral half-spreading angle increased by a factor of about three compared to an isolated spot.

Previous experimental results were based on ensemble-averaged flow measurements and planar visualisation images. A complete picture of the flow field can be obtained using DNS, which may facilitate the interpretation of the complex three-dimensional structure of a spot. The present computations are primarily carried out to improve our understanding of the physics associated with the merging of turbulent spots in a supersonic boundary layer flow.

2. Spot simulations

2.1. Numerical approach

The unsteady compressible Navier–Stokes (N–S) equations for dimensionless density ρ, velocity u_i, pressure p, temperature T and total energy E, in cartesian coordinates are

$$\frac{\partial \rho}{\partial t}+\frac{\partial \rho u_j}{\partial x_j}=0 \tag{1}$$

$$\frac{\partial \rho u_i}{\partial t}+\frac{\partial \rho u_i u_j}{\partial x_j}=-\frac{\partial p}{\partial x_i}+\frac{1}{Re}\frac{\partial \tau_{ij}}{\partial x_j} \tag{2}$$

$$\frac{\partial E}{\partial t}+\frac{\partial (E+p)u_j}{\partial x_j}=\frac{\partial u_i \tau_{ij}}{\partial x_j}+\frac{1}{(\gamma-1)RePrM^2}\frac{\partial}{\partial x_j}\left(\mu\frac{\partial T}{\partial x_j}\right) \tag{3}$$

where the stress is given by

$$\tau_{ij}=\mu\left(\frac{\partial u_j}{\partial x_i}+\frac{\partial u_i}{\partial x_j}-\frac{2}{3}\delta_{ij}\frac{\partial u_k}{\partial x_k}\right) \tag{4}$$

The temperature is given by

$$T=\gamma(\gamma-1)M^2\left(\frac{E}{\rho}-\frac{1}{2}u_i u_j\right) \tag{5}$$

The equation of state can be written as

$$p=(\gamma-1)\left(E-\frac{1}{2}\rho u_i u_j\right)=\frac{1}{\gamma M^2}\rho T \tag{6}$$

The non-dimensional parameters governing the flow are Reynolds number; $Re = \rho_r^* u_r^* x_r^* / \mu_r^*$, Mach number; $M = u_r^* / \sqrt{\gamma R^* T_r^*}$, ratio of specific heats; $\gamma = c_p/c_v$, and Prandtl number; $Pr = \mu_r^* c_p^* / k^*$ which is set to 0.72. The variation of the dynamic viscosity with temperature is accounted for by using a power law $(\mu^*/\mu_r^* = (T^*/T_r^*)^{\omega})$ with a constant $\omega = 2/3$. In the above expressions the subscript r denotes a reference value and asterisks (*) represent dimensional variables.

2.2. Entropy-splitting

The governing equations are solved using a stable high-order scheme. An entropy splitting approach is used to split the Euler terms into conservative and non-conservative parts. Consider a system of hyperbolic conservation equations of the form

$$u_t + f_x = 0 \tag{7}$$

where u and f are column vectors. Applying the entropy variable transformation using the split high-order entropy conserving scheme of Gerritsen and Olsson (1998) gives

$$u_w w_t + f_w w_x = 0 \tag{8}$$

The final split form can be written as

$$\frac{\beta}{\beta+1} u_t + \frac{1}{\beta+1} u_w w_t + \frac{\beta}{\beta+1} f_x + \frac{1}{\beta+1} f_w w_x = 0; \quad \beta \neq -1 \tag{9}$$

where β is a splitting parameter. The original un-split conservative form can be recovered as $\beta \to \infty$. In the present simulation the value of β was set to 4.0 (Sandham et al., 2002). All the spatial discretizations are carried out using a fourth-order central-difference scheme while the time integration uses a third-order Runge–Kutta method. A stable boundary scheme of Carpenter et al. (1999), along with a Laplacian formulation of the viscous and heat conduction terms, are used to prevent the odd–even decoupling associated with central schemes. An artificial compression method (ACM) variant of a standard total variation diminishing (TVD) family is used to capture flow discontinuities (shock waves). The TVD filter is applied at the end of each full time step in the form of an additional numerical flux term

$$F_{j+\frac{1}{2}} = R_{j+\frac{1}{2}} \Phi_{j+\frac{1}{2}} \Psi_{j+\frac{1}{2}} \tag{10}$$

where R is the right eigenvector matrix of the flux Jacobian from the Euler equations and Φ is defined by the TVD scheme. Ψ is a sensor (Ducros et al., 1999) which takes low values where the flow is turbulent and values close to one in the vicinity of a shock

$$\Psi = \frac{(\mathrm{div}(V))^2}{(\mathrm{div}(V))^2 + (\mathrm{rot}(V))^2 + \epsilon} \tag{11}$$

where V is the velocity vector and ϵ is machine zero.

More details regarding the entropy-splitting and other numerical issues used in the present scheme can be found in Sandham et al. (2002).

Table 1
Details of spot simulations

Case	$(L_x, L_y, L_z)/\delta_{in}^*$	N_x, N_y, N_z
Single (M2I)	$400 \times 60 \times 60$	$801 \times 101 \times 121$
Lateral (M2LM)	$400 \times 60 \times 100$	$801 \times 101 \times 201$
Tandem (M2TM)	$400 \times 60 \times 60$	$801 \times 101 \times 121$

$M_\infty = 2.0$, $Re_{\delta_{in}^*} = 950.0$, $T_w = 1.672 T_\infty$.

2.3. Flow configuration

All lengths are normalised with the displacement thickness (δ_{in}^*) of the laminar inflow profile. The laminar base flow is obtained by a separate self-similar compressible boundary layer solution. Details of the various test cases considered are given in Table 1. For the present flow conditions an unperturbed laminar base flow remained laminar. The flow domain is discretized using an equally spaced grid along the streamwise (x) and spanwise (z) directions and a stretched grid in the wall normal (y) direction. The estimated streamwise and spanwise grid resolutions in viscous wall units are Δx^+, $\Delta z^+ = 9$–11 based on the maximum local mean[1] friction velocity $(u_\tau = \sqrt{\mu_w (\mathrm{d}u/\mathrm{d}y)_w / \rho_w}$, with subscript w denoting the wall). The minimum grid spacing in the wall-normal direction is $\Delta y^+ = 0.89$ and 11 points are used in the sub-layer region $(y^+ < 10)$ and 27 points within $y^+ < 30$. In the supersonic part of the inflow boundary all the properties are fixed, while in the subsonic region the pressure is extrapolated from the interior. Characteristic non-reflective conditions (Thompson, 1987) at the outlet, integrated characteristic boundary condition (whereby outgoing characteristics are numerically integrated in time and added to prescribed free stream conditions) at the top surface and a no-slip, isothermal condition at the flat plate surface are imposed as boundary conditions. Periodic boundary conditions are applied in the spanwise direction. First the laminar base flow is allowed to develop along the plate until steady-state conditions are reached. The spatially developed laminar base flow is perturbed by a localised blowing through the flat plate surface. A spanwise-symmetric rectangular slot of dimensions 4×4 (x, z) is used. The blowing trip is activated for a short duration of eight non-dimensional time units (δ_{in}^*/u_∞) by specifying vertical velocity at the plate surface as

$$v_{in\,j} = A u_\infty \text{ for } \begin{cases} 20 \leqslant x \leqslant 24, \;\; 28 \leqslant z \leqslant 32, \;\; t < 8 \text{ (M2I)} \\ 36 \leqslant z \leqslant 40; \;\; 60 \leqslant z \leqslant 64, \;\; t < 8 \text{ (M2LM)} \\ 28 \leqslant z \leqslant 32; \;\; t < 8, \;\; 98 < t < 106 \text{ (M2TM)} \end{cases}$$

The amplitude of the disturbance was chosen as $A = 0.20$ such that a spot can be triggered (Elder, 1960) and tracked within the present domain size. Other amplitudes and spot triggering methods have been employed in

[1] Mean properties refers to the spanwise-averaged flow properties in the spot core (averaged over $20 \leqslant z \leqslant 40$).

Krishnan (2005); the mature spot properties appear to be independent of the spot initiation method.

3. Results and discussion

In this section the results for a single turbulent spot are summarized first and then the dynamics of spot merging are discussed in detail.

3.1. Single spot dynamics

Coherent structures in the flow are identified by calculating the second invariant $\left(\Pi = \frac{\partial u_i}{\partial x_j}\frac{\partial u_j}{\partial x_i}\right)$ of the velocity gradient tensor. Negative values of Π correspond to regions in the flow where the vorticity dominates over strain. The injected low momentum fluid acts as a blockage to the flow and induces hairpin vortices downstream of the injection slot. These primary hairpin structures are stretched by the mean flow shearing action and are convected downstream. Fig. 3 shows the structure at $t = 36$, with a primary hairpin vortex surrounded by evolving second-generation structures. The strength of the primary structures is high due to the large amplitude blowing trip and they trigger secondary hairpin structures, quasi-streamwise vortices and other auxiliary structures in the flow by a vortex regeneration mechanism (Haidari and Smith, 1994). As they are convected downstream, the structures grow and their interaction finally evolves into a localised turbulent patch i.e. a turbulent spot. A turbulent spot at time $t = 451$ is shown in Fig. 4 with surfaces of constant wall-normal vorticity. This clearly shows the arrowhead shaped front overhang, lateral wingtips and the longitudinal vortices around the tail interface and is similar to the classical spot sub-layer flow visualisation pictures of Cantwell et al. (1978) shown in Fig. 2. A semi-log plot of the mean velocity profiles at different

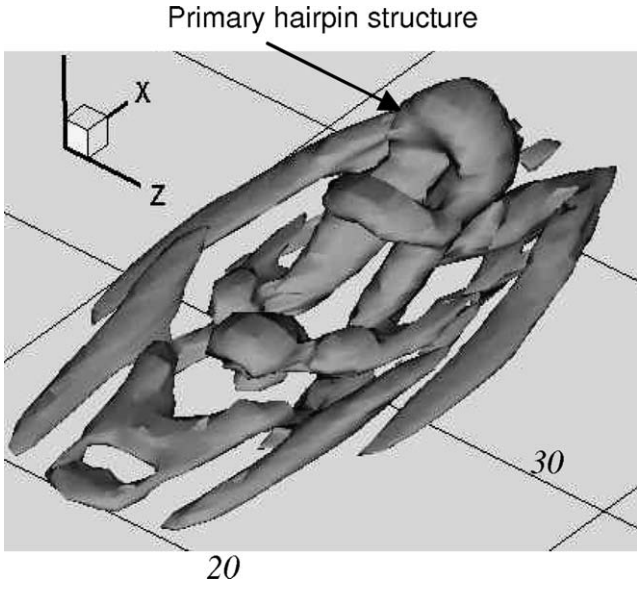

Fig. 3. Coherent structures downstream of the injection slot (case M2I), $t = 36$, surface of second invariant $\Pi = -0.002$.

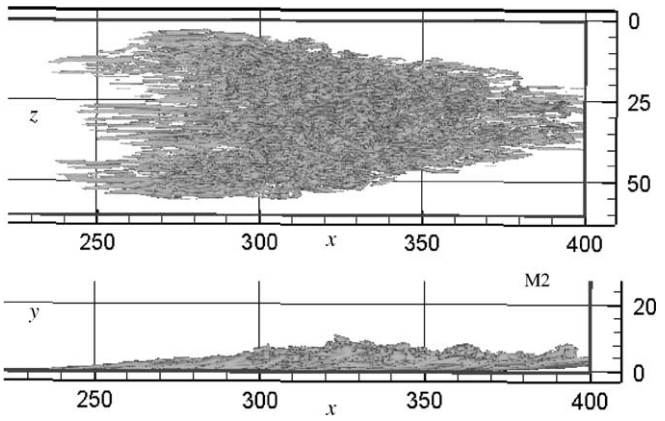

Fig. 4. Iso surface of wall-normal vorticity, (case M2I); $t = 451$, $\omega_y = \pm 0.06$. Upper figure: plan view. Lower figure: side view.

streamwise locations along the spot core at time $t = 451$ (Fig. 5(a)) and the corresponding turbulent fluctuations shown in Fig. 5(b) illustrate the existence of a well developed turbulent region inside the spot.

Isolated spot simulations (Krishnan and Sandham, 2004b) showed that the spanwise extremities at the rear of the spot (the lateral wingtips) are accompanied by a defect in streamwise velocity. These velocity-defect regions are caused by the upwash of near-wall fluid by coherent structures in the wingtip region. This can be explained after we note that the high momentum turbulent fluid inside the spot is surrounded by the low speed laminar fluid. This creates a lateral shear ($\partial u/\partial z$) along the wingtips, the strength of which will depend on the difference between the turbulent profile within the spot and the laminar profile outside it. The rollers induced by the lateral shear are tilted in the streamwise direction by the mean shear, leading to a quasi-streamwise structure which cause an upwash of near-wall fluid in the wingtip region. A detailed schematic of the proposed destabilising mechanism responsible for the lateral spreading of the spot is given in Fig. 6. The velocity-defect regions are unstable and break down quickly to turbulence, resulting in a spreading of the spot.

This mechanism based on lateral shear can be used to explain the qualitative variation in spot spreading rate in a variety of flows, such as the inhibition of the lateral growth of spots in a boundary layer with a favourable pressure gradient (where the lateral shear is reduced), enhanced growth in an adverse pressure gradient flow, suppression of the spot growth during the interaction with a turbulent boundary layer and the effects of compressibility. A more elaborate discussion is provided in Krishnan (2005).

A three-dimensional plan view of the wall-normal vorticity at a threshold value of ± 0.06 is used to locate the spot boundary at different times during the spot evolution. The axial locations of the spot front, tail and the maximum half-width ($b_{\frac{1}{2}}$) at various time instants are used to calculate the spot celerities. The spot features are found to propagate with constant speeds during the self-similar growth of the spot (Krishnan and Sandham, 2004b). The lateral

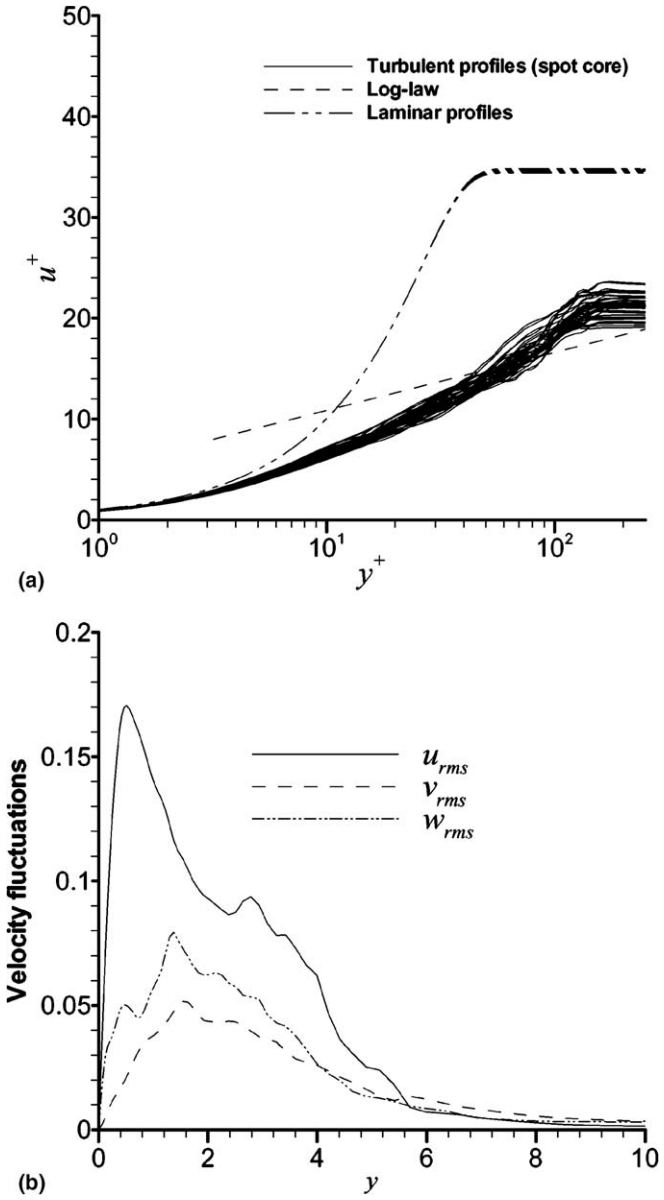

Fig. 5. (a) Mean streamwise velocity distribution in the spot core $310 \leqslant x \leqslant 330$ for the isolated spot case M2I at time $t = 451$, dashed line – law of the wall: $u^+ = 2.5 * \ln(y^+) + 5.1$, (b) mean velocity fluctuations at $x = 299.5$.

half-spreading angle (defined as $\beta = \tan^{-1}(\mathrm{d}b_{\frac{1}{2}}/\mathrm{d}x)$, where $b_{\frac{1}{2}}$ is the maximum half-width of the spot) in the present Mach 2 flow is estimated as 5°, compared to the spreading angle of incompressible spots, which is in the range of 8.5–11°. This reduction in growth rate due to compressibility is consistent with the experimental data of Fischer (1972). The front of the spot is convected at $0.87u_\infty$ and the tail at $0.53u_\infty$. The corresponding front and tail speeds of incompressible spots reported in the literature are in the range of 0.85–0.9 and 0.5–0.6, respectively, so the compressibility can be seen to have a very strong effect on spreading angle, but apparently only a small effect on spot convection speeds, at least up to $M = 2$.

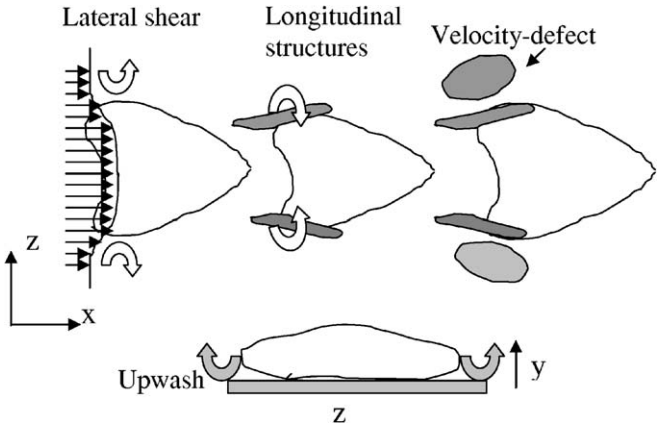

Fig. 6. Schematic of the proposed lateral destabilising mechanism of the spot.

3.2. Lateral merging

Fig. 7 shows a three-dimensional view of the spots during an early stage of the lateral merging process. Spot substructures, consisting of hairpin-shaped and quasi-streamwise vortices may be seen inside the spot. Iso-surfaces of the streamwise velocity perturbations (relative to the laminar profile: $u' = u - u_1$) shown in Fig. 8 (plan view) and Fig. 9 (side view) indicate a strong velocity defect in the interaction region. The formation of a calmed region at the rear of the spot is also visible as a velocity excess region, shown with the lighter surface contour. Fig. 10 shows the streamwise variation of the wall-normal velocity in the defect region at $t = 173$. It can be seen that the wall-normal velocity near the interacting wingtips is almost two times higher than near the free wingtips. A schematic of this process is shown in Fig. 11. The spot interaction triggers highly unstable inflectional velocity profiles away

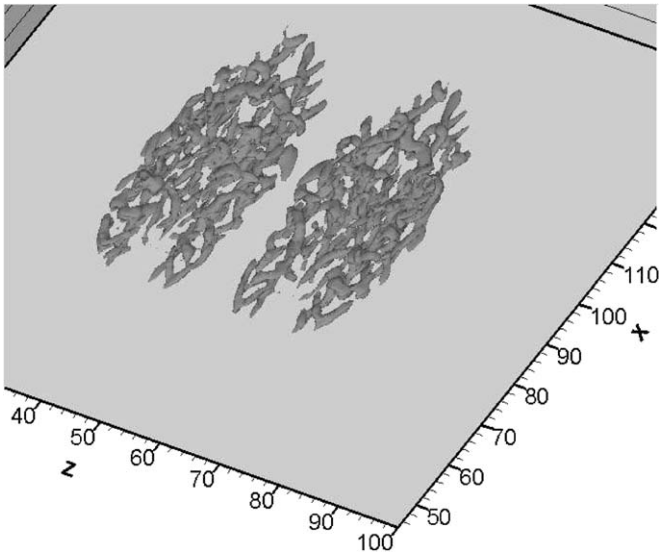

Fig. 7. Iso contours of second invariant $\Pi = -0.002$ showing the spot substructures at $t = 130$.

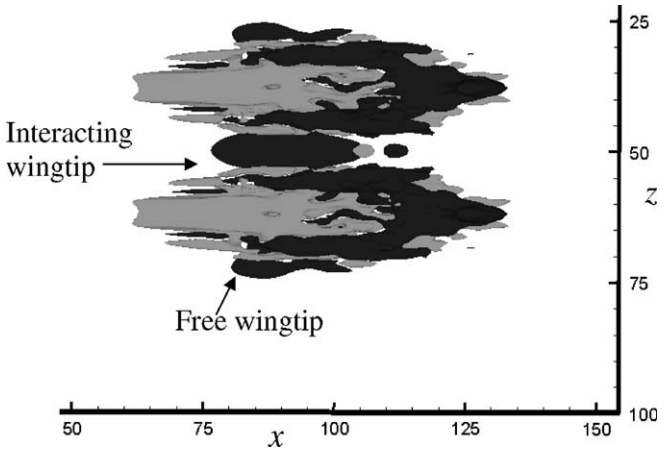

Fig. 8. Plan view showing iso-contours of streamwise velocity perturbations $u' = \pm 0.02$ at $t = 130$.

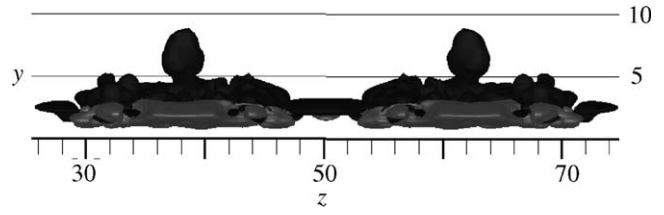

Fig. 9. Side view showing iso-contours of streamwise velocity perturbations ($u' = \pm 0.02$, $t = 130$); dark shade: velocity defect region, light shade: velocity excess region.

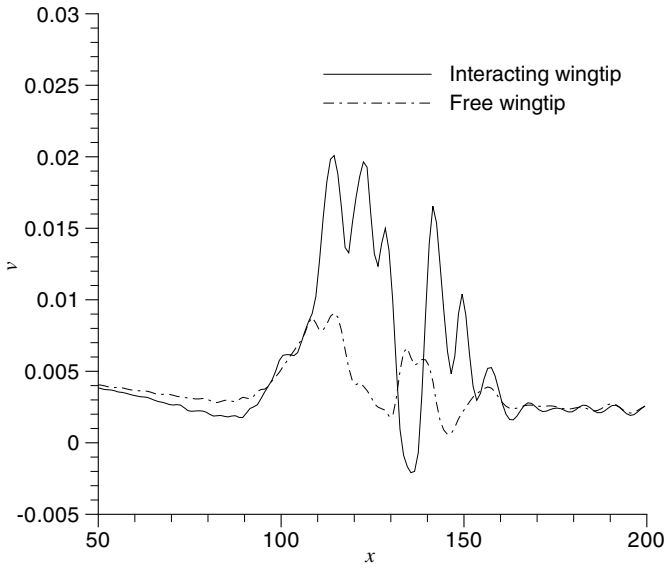

Fig. 10. Comparison of the wall-normal velocity distribution at $y = 2.932$, and $t = 173$. Free wingtip: $z = 25$, interacting wingtip: $z = 50$.

from the wall, as shown in Fig. 12. This inflectional instability generates new coherent structures which connect the two spots in the wingtip region. These new structures have a hairpin shape and can be seen in the region $210 \leqslant x \leqslant 240$ on the centreline, $z = 50$, in Fig. 13.

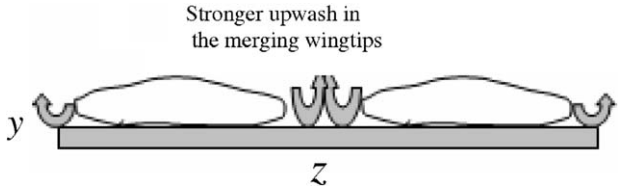

Fig. 11. Schematic outline of spot merging.

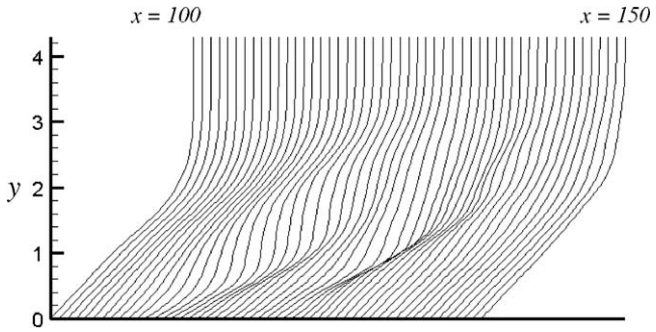

Fig. 12. Inflectional streamwise velocity profiles in the merging zone $t = 173$, $z = 50$.

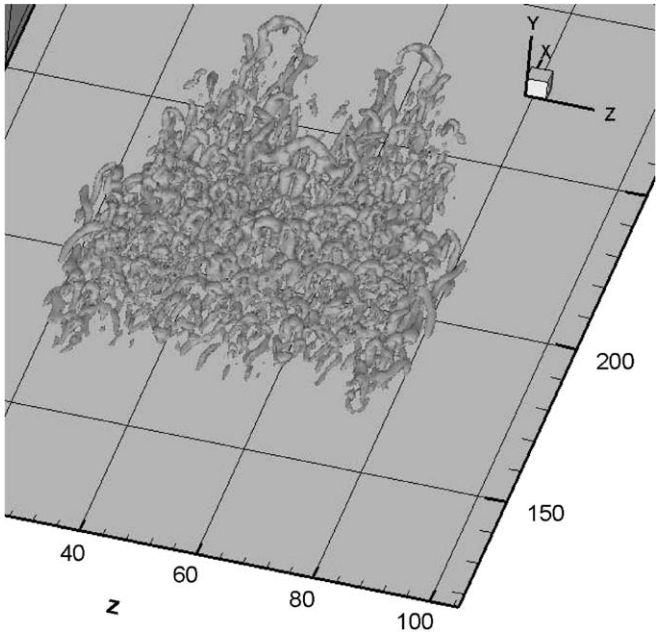

Fig. 13. Contours of second invariant $\Pi = -0.002$ showing the evolved coherent structures during the spot merging at $t = 290$.

3.3. Intermittency distribution

The fraction of time a point on the surface experiences turbulent motion due to the passage of a turbulent spot is defined as the intermittency γ. Dhawan and Narasimha (1958) successfully calculated the local skin friction distribution during transition, c_{ft}, using intermittency data from

experiments. They assumed that the skin friction during transition can be represented as a linear combination of the corresponding laminar c_{fL} and the turbulent skin friction c_{fT} values as

$$c_{ft} = (1-\gamma)c_{fL} + \gamma c_{fT} \tag{12}$$

From the DNS results we know the laminar skin friction distribution and the transitional skin friction value. The turbulent skin friction value is obtained using the Eckert (1955) correlation based on the reference temperature method as

$$c_{fT} = \frac{0.370}{[\log_{10}(Re_x/(\rho^R\mu^R))]^{2.584}},$$
$$c_{fL} = \frac{0.664}{\sqrt{(Re_x/(\rho^R\mu^R))}} \tag{13}$$

A reference temperature: $T^R = T_e + 0.5(T_w - T_e) + 0.22(T_{rec} - T_e)$ is used to calculate the density (ρ^R) and the viscosity (μ^R) used in the correlations. T_{rec} is the adiabatic recovery temperature, T_e is the temperature at the outer edge of the boundary layer and T_w is the temperature at the wall. Comparison of the present laminar skin friction value with the Eckert (1955) laminar correlation showed excellent agreement. The local intermittency distribution of the spot is estimated by solving Eq. (12) for γ. The intermittency distribution at the flat plate surface at time $t = 290$ is plotted in Fig. 14. Higher values of γ are seen near the free wingtips and the interaction region. This reflects the high skin friction associated with the newly generated turbulence. The complex interaction dynamics of the spots should be taken into account for the development of accurate intermittency based transition models capable of predicting transitional flow properties.

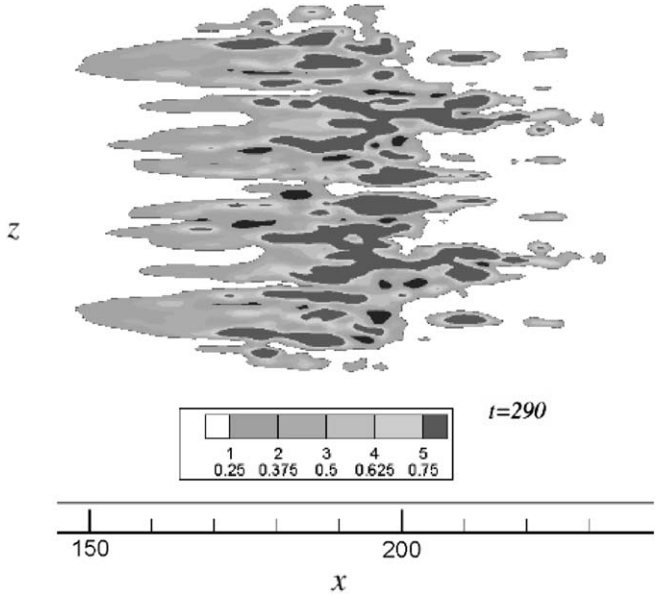

Fig. 14. Intermittency distribution at $t = 290$.

3.4. Tandem merging

The inline (tandem) merging of two spots is different to the lateral merging case of the previous section since there is a calmed region behind the spot. The influence of the calmed region of the downstream spot on the growth of the upstream spot is addressed in this section. Iso-contours of the streamwise velocity perturbations at $t = 134$ are plotted in Fig. 15. This shows how the upstream spot enters the calmed region of the downstream spot. This calmed region has fuller velocity profiles and hence a strong stabilising effect on the upstream spot. Further downstream the overhang region of the upstream spot is found to overtake the tail of the downstream spot, since the front overhang is travelling at a convection speed of about $0.87u_\infty$. The leading edge hairpin structure of the upstream spot can still be identified in the merged region, as seen in Fig. 16, which shows surfaces of constant Π. The lateral growth of the upstream spot is seen to be reduced relative to that of an isolated spot. The intermittency distribution, shown in Fig. 17, confirms the suppressed growth of the upstream spot. Further downstream at $t = 450$, Fig. 18 indicates that the upstream spot has been trapped inside the downstream spot. The dashed line marks the boundary of the upstream spot, in which individual structures can still be tracked. Due to the interaction the celerity of the downstream spot is not altered. However, the influence of its calmed region on the dynamics of the upstream spot is significant. This

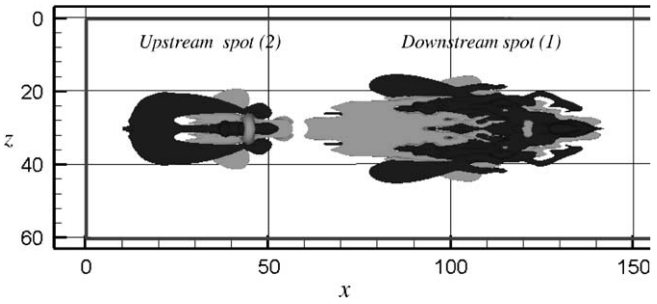

Fig. 15. Streamwise velocity perturbations at $t = 134$, $u' = \pm 0.02$; dark shade: velocity defect region, light shade: velocity excess region.

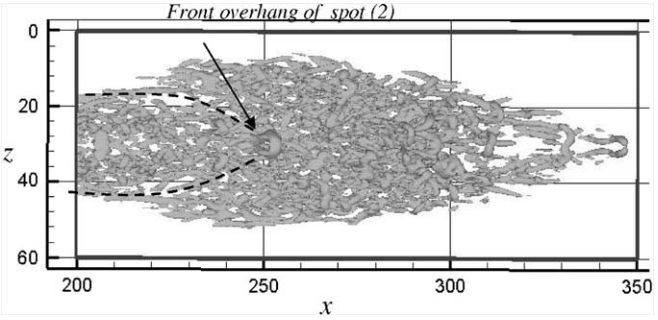

Fig. 16. Coherent structures showing the interaction of the upstream spot with the tail of the downstream spot, $t = 374$, $\Pi = \pm -0.002$. The dashed line shows the approximate location of the upstream spot.

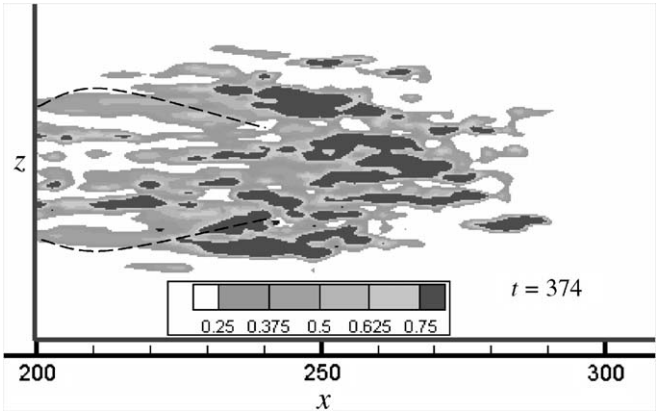

Fig. 17. Intermittency distribution during tandem merging of spots at $t = 374$. The dashed line shows the approximate location of the upstream spot.

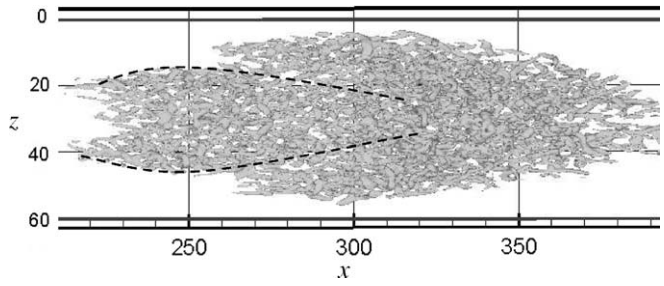

Fig. 18. Coherent structures showing the interaction of the upstream spot with the tail of the downstream spot, $t = 450$, $\Pi = \pm -0.002$. The dashed line shows the approximate location of the upstream spot.

process is consistent with the experiments of Gutmark and Blackwelder (1987), who noticed a reduction in the celerities of the upstream spot with a decrease in the time delay between the generation of spots in an incompressible flow.

There are also similarities with Zilberman et al. (1977), who initiated a turbulent spot in a laminar boundary layer and allowed it to interact with a turbulent boundary layer downstream. They noticed large scale structures evolving from the interactions and also found a drastic reduction in the lateral and streamwise growth of the spot. In this case the velocity difference across the wingtips is reduced, since the surrounding turbulent fluid is travelling at a faster speed. This in turn reduces the lateral shear and the spot destabilisation process i.e. a weak upwash near the wingtips.

4. Summary

The dynamics of an isolated turbulent spot, together with lateral and tandem merging of spots in a supersonic boundary layer have been studied in detail by DNS. An array of hairpin-shaped and quasi-streamwise vortices are identified as the main spot substructures. Coherent structures in the wingtip region destabilise the surrounding laminar fluid by displacing the near-wall fluid away from the surface (upwash) and were found to be responsible for the lateral growth of the spot. In the lateral merging of spots a strong velocity-defect region is created in the interaction zone due to the combined upwash associated with the wingtip structures. The effect is twice as large as in an isolated spot. Inflectional velocity profiles associated with the velocity defect trigger new large scale structures in the interaction zone. For tandem merging of spots it was found that the growth of the upstream spot was highly suppressed in the calmed region of a downstream spot.

Acknowledgements

The authors would like to acknowledge the financial support of the European Space Agency (ESA-ESTEC) for this work, under contract 17531/03/NL/SFe, technical officer Dr. J. Steelant.

References

Cantwell, B., Coles, D., Dimotakis, P., 1978. Structure and entrainment in the plane of symmetry of a turbulent spot. J. Fluid Mech. 87, 641–672.

Carpenter, M.H., Nordstrom, J., Gottlieb, D., 1999. A stable and conservative interface treatment of arbitrary spatial accuracy. J. Comp. Phys. 148, 341–365.

Dhawan, S., Narasimha, R., 1958. Some properties of boundary layer flow during transition from laminar to turbulent motion. J. Fluid Mech. 3, 418–436.

Ducros, F., Ferrand, V., Nicoud, F., Weber, C., Darracq, D., Gacherieu, C., Poinsot, T., 1999. Large-Eddy simulation of the shock/turbulence interaction. J. Comp. Phys. 152, 517–549.

Eckert, E.R.G., 1955. Engineering relations for skin friction and heat transfer to surfaces in high velocity flows. J. Aero. Sci. 22, 585–587.

Elder, J.W., 1960. An experimental investigation of turbulent spots and breakdown to turbulence. J. Fluid Mech. 9, 235–246.

Emmons, H.W., 1951. The laminar-turbulent transition in a boundary layer. J. Aero. Sci. 18, 490–498.

Fischer, M.C., 1972. Spreading of a turbulent disturbance. AIAA J. 10 (7), 957–959.

Gerritsen, M., Olsson, P., 1998. Designing an efficient solution strategy for fluid flows: 1. A stable high order finite difference scheme and sharp shock resolution for the Euler equations. J. Comp. Phys. 129, 245–262.

Gutmark, E., Blackwelder, R.F., 1987. On the structure of a turbulent spot in a heated laminar boundary layer. Exp. Fluids 5, 217–229.

Haidari, A.H., Smith, C.R., 1994. The generation and regeneration of single hairpin vortices. J. Fluid Mech. (277), 135–162.

Henningson, D.S., Spalart, P., Kim, J., 1987. Numerical simulations of turbulent spots in plane Poiseuille and boundary-layer flow. Phy. Fluids 30 (10), 2914–2917.

Jacobs, R.G., Durbin, P.A., 2001. Simulations of bypass transition. J. Fluid Mech. 428, 185–212.

Krishnan, L., 2005. Dynamics of turbulent spots in a compressible flow, PhD Thesis, University of Southampton.

Krishnan, L., Sandham, N.D., 2004a. Large eddy simulation of compressible turbulent spots. Advances in Turbulence X. CIMNE, Barcelona, pp. 467–471.

Krishnan, L., Sandham, N.D., 2004b. Turbulent spots in a compressible boundary-layer flow. In: IUTAM Symp. on Laminar-Turbulent Transition.

Krishnan, L., Sandham, N.D., 2004c. Turbulent spot/separation bubble interactions in a spatially evolving supersonic boundary layer flow. Enhancement of NATO Military Flight vehicle Performance by Management of Interacting Boundary Layer Transition and Separation, RTO-MP-AVT-111, 27, 1–15.

Makita, H., Nishizawa, A., 2001. Characteristics of internal vortical structures in a merged turbulent spot. J. Turbulence 2 (12), 1–16.

Narasimha, R., 1985. The laminar-turbulent transition zone in the boundary layer. Prog. Aero. Sci. 22, 81–111.

Sandham, N.D., Li, Q., Yee, H.C., 2002. Entropy splitting for higher-order numerical simulation of compressible turbulence. J. Comp. Phys. 178, 307–322.

Savas, O., Coles, D.E., 1985. Coherence measurements in synthetic turbulent boundary layers. J. Fluid Mech. 160, 421–446.

Schubauer, G.B., Klebanoff, P.S., 1955. Contribution on the mechanics of boundary-layer transition. NACA Tech. Note 3489.

Thompson, K.W., 1987. Time dependent boundary conditions for hyperbolic systems. J. Comp. Phys. 68, 1–24.

Zilberman, M., Wygnanski, I., Kaplan, R.E., 1977. Transitional boundary layer spot in a fully turbulent environment. Phys. Fluids 20, S258–S271.